

Maximum-Likelihood Sequence Detector for Dynamic Mode High Density Probe Storage

Naveen Kumar*, Pranav Agarwal†, Aditya Ramamoorthy* and Murti Salapaka†

*Dept. of Electrical and Computer Engineering

Iowa State University, Ames, IA 50010

Email: nk3,adityar@iastate.edu

†Dept. of Electrical and Computer Engineering

University of Minnesota, Minneapolis, MN 55455

Email: agar0108,murtis@umn.edu

Abstract— There is an ever increasing need for storing data in smaller and smaller form factors driven by the ubiquitous use and increased demands of consumer electronics. A new approach of achieving a few Tb per in² areal densities, utilizes a cantilever probe with a sharp tip that can be used to deform and assess the topography of the material. The information may be encoded by means of topographic profiles on a polymer medium. The prevalent mode of using the cantilever probe is the static mode that is known to be harsh on the probe and the media. In this paper, the high quality factor dynamic mode operation, which is known to be less harsh on the media and the probe, is analyzed for probe based high density data storage purposes. It is demonstrated that an appropriate level of abstraction is possible that obviates the need for an involved physical model. The read operation is modeled as a communication channel which incorporates the inherent system memory due to the inter-symbol interference and the cantilever state that can be identified using training data. Using the identified model, a solution to the maximum likelihood sequence detection problem based on the Viterbi algorithm is devised. Experimental and simulation results demonstrate that the performance of this detector is several orders of magnitude better than the other existing schemes and confirm performance gains that can render the dynamic mode operation feasible for high density data storage purposes.

I. INTRODUCTION

The rapid growth in the personal computer industry and the Internet is a major factor underlying the demand for ultra-high capacity storage devices. Demands of a few Tb per in.² are predicted in the near future. Currently storage systems are mainly based on magnetic, optical and solid state technologies. However all these technologies are reaching fundamental limits on their achievable areal densities.

A promising high density storage methodology, that is the focus of this paper utilizes a sharp tip at the end of a micro cantilever probe to create (or remove) and read indentations (see [15] for an example). Recently, experimentally achieved tip radii near 5 nm on a micro-cantilever were used to create areal densities close to 4 Tb/in² [7], [1]. The presence/absence of an indentation represents a bit of information. The main advantage of this method is the significantly higher areal densities that are possible. The work of [15], [8] uses the static mode operation of the atomic force microscope (AFM)

where the cantilever's operation is in contact mode which degrades the medium and the probe. In the dynamic mode operation given in this paper, the cantilever with a high quality factor is forced sinusoidally using a dither piezo and it gently taps on the medium intermittently which reduces the medium and the probe wear [16]. High quality factor cantilevers are desirable for a dynamic mode operation because the effect of a topographic change on the medium, on the oscillating cantilever, lasts much longer (approximately Q cycles where Q is the quality factor) and the signal to noise ratio increases with higher quality factors (improves as \sqrt{Q} [12]). However, the advantages of high quality factor with respect to resolution become disadvantages with respect to bandwidth which is apparent as the effect of a topographic change lasts longer and therefore information on the medium has to be temporally spaced to reduce inter-symbol interference. Thus the challenges of designing good detection schemes are twofold; the first is that of modeling that remains tractable for a data storage purpose which might not encapsulate the entirety of the behavior inherent in the dynamic mode but remains useful for detecting information stored on the medium and the second is to use the model to exploit the advantages of high quality factor cantilevers without sacrificing bandwidth. Both these challenges are met in this paper and the results are corroborated with experimental results.

The cantilever dynamics is complex with a number of physical intricacies that can render the modeling of the dynamic mode intractable for high performance data storage purposes. In this paper, it is demonstrated that an appropriate level of abstraction is possible that obviates the need for an involved physical model. The dynamic mode read operation is modeled as a communication channel model which incorporates the inherent system memory due to the inter-symbol interference and the cantilever state that can be identified using training data. Using the identified model, a solution to the maximum likelihood sequence detection problem based on the Viterbi algorithm is devised. Experimental and simulation results corroborate the analysis of the detector, demonstrate that the performance of this detector is several orders of magnitude better than the performance of other existing schemes and confirm performance gains that can render the dynamic mode operation feasible for high density data storage purposes.

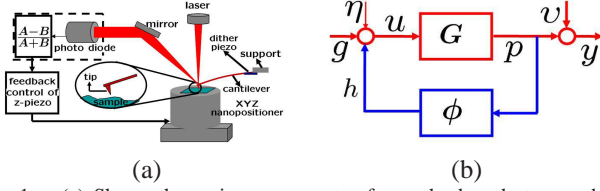


Fig. 1. (a) Shows the main components of a probe based storage device. (b) Shows a block diagram representation of the cantilever system G being forced by white noise (η), tip-media force h and the dither forcing g . The output of the block G , the deflection p is corrupted by measurement noise v that results in the measurement y . Tip media force $h = \phi(p)$.

The paper is organized as follows. In Section II, background and related work of the probe based data storage system is presented. Section III deals with the problem of designing and analyzing the data storage unit as a communication system and finding efficient detectors for the channel model. Section IV and Section V report results from simulation and experiments respectively. Section VI summarizes the main findings of this paper and provides the conclusions and future work.

II. BACKGROUND AND RELATED WORK.

In the standard atomic force microscope setup, which has formed the basis of probe based data storage, the cantilever deflection is measured by a beam-bounce method where a laser is incident on the back of the cantilever surface and the laser is reflected from the cantilever surface into a split photodiode (see Figure 1(a)). The advantage of the beam-bounce method is the high resolution (low measurement noise) and high bandwidth (in the 2-3 MHz) range. The disadvantage is that it is more cumbersome for integrating this method into a parallel operation where multiple cantilevers operate in parallel. There are attractive measurement mechanisms that integrate the cantilever motion sensing onto the cantilever itself. These include piezo-resistive sensing [4] and thermal sensing [6]. For the dynamic mode operation there are various schemes to actuate the cantilever that include electrostatic [5], mechanical by means of a dither piezo that actuates the support of the cantilever base and magnetic [9]. In this paper, it is assumed that the cantilever is actuated by a dither piezo and the sensing mechanism employed is the beam bounce method (see Figure 1(a)). Even though the experimental setup reported in this paper uses a particular scheme of detection and actuation of the cantilever, the paradigm developed for data detection is largely applicable in principle to other modes of detection and actuation of the cantilever. For channel modeling purposes, the AFM dynamics is viewed in the systems perspective as an interconnection of a linear cantilever system with the nonlinear tip-media interaction forces (ϕ) in feedback (See Figure 1(b)). The interaction forces ϕ depend on the tip deflection p [13].

A. Cantilever-Observer Architecture

As mentioned earlier, the high Q cantilever gives high signal to noise ratio and less tip-media wear but it is limited in bandwidth. The quality factor of the cantilever can be reduced to fasten the decay of the transient resulting in higher bandwidth. However, low Q operation results in lower resolution and higher forces. This tradeoff between resolution and bandwidth can be well tackled by using the cantilever-observer framework shown in Figure 2. The cantilever-observer framework decouples the bandwidth from Q allowing one to use a high

Q system giving better resolution and high bandwidth at the same time [12]. It gives the flexibility to shorten the impulse response of the channel and cancels the effect of the dither at the output. In this framework, the error process is denoted by e which is the actual deflection signal minus the estimated deflection signal. With the dither input (g), thermal noise (η), measurement noise (v) and the observer with Kalman gain, the error process e approaches a zero mean wide sense stationary stochastic process when $\phi = 0$ i.e. no tip-media interaction is present [12]. If ϕ is neglected from the system, the system from the dither input (g) to error process (e) can be modeled as a linear system whose impulse response is denoted by $\Gamma(t)$ with zero mean white Gaussian noise $n(t)$ with variance V which is characterized by thermal and measurement noise (See Figure 3).

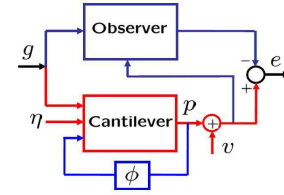


Fig. 2. An observer architecture for the system in Figure 1(b)

III. CHANNEL MODEL AND DETECTORS

The cantilever based data storage system can be modeled as a communication channel as shown in Figure 3. The components of this model are explained below in detail.

Shaping Filter ($b(t)$): The model takes as input the bit sequence ($a_0, a_1 \dots a_{N-1}$) where $a_k, k = 1, \dots, N-1$ is equally likely to be 0 or 1. In the probe storage context, '0' refers to the topographic profile being *low* and '1' refers to the topographic profile being *high*. Each bit has a duration of T seconds. This duration can be found based on the length of the topographic profile specifying a single bit and the speed of the scanner. The height of the high bit is denoted by A . The cantilever interacts with the media by gently tapping it when it is high. When the media is low, typically no interaction takes place. We model the effect of the medium height using a filter with impulse response $b(t)$ (shown in Figure 3) that takes as input, the input bit impulse train $a(t) = \sum_{k=0}^{N-1} a_k \delta(t - kT)$. The output of the filter is given by $\check{a}(t) = \sum_{k=0}^{N-1} a_k b(t - kT)$ which is high/low when the corresponding bit is '1'/'0'.

Nonlinearity Block (ϕ): The cantilever oscillates at frequency f_c which means that in each cantilever cycle of duration $T_c (= 1/f_c)$, the cantilever hits the media at most once if the media is high during a time T_c . In each high bit duration T , the cantilever hits the media q times (i.e. $T = qT_c$) with varying magnitudes. Therefore, for N bits, the output of the nonlinearity block is given by, $\tilde{a}(t) = \sum_{k=0}^{Nq-1} \nu_k(\tilde{a}) \delta(t - kT_c)$, where ν_k denotes the magnitude of the k^{th} impact of the cantilever on the medium. We are approximating the nonlinearity block output as a sequence of impulsive force inputs to the cantilever. The strength of the impulsive force inputs are dependent on previous impulsive hits; precisely because the previous interactions affect the amplitude of the oscillations that in turn affect how hard the hit is at a particular instant of time. The exact dependence is very hard to model

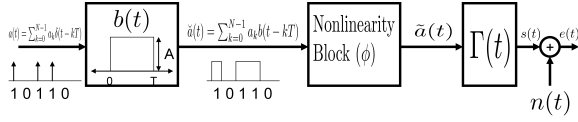


Fig. 3. Continuous time channel model of probe based data storage system deterministically and therefore we chose a Markov model for the sequence of impact magnitudes for a single bit duration,

$$\bar{\nu}_i = \bar{\Theta}(a_i, a_{i-1}, \dots, a_{i-m}) + \bar{b}_i \quad (1)$$

where $\bar{\nu}_i = [\nu_{iq} \ \nu_{iq+1} \dots \nu_{(i+1)q-1}]^T$, $\bar{\Theta}(a_i, a_{i-1}, \dots, a_{i-m})$ is a function of current and last m bits, m denotes the inherent memory of the system and \bar{b}_i is a zero mean i.i.d. Gaussian vector of length q .

Channel Response ($\Gamma(t)$): The Markovian modeling of the output of the nonlinearity block as discussed above allows us to break the feedback loop in Figure 2. The rest of the system can then be modeled by treating it as a linear system with impulse response $\Gamma(t)$. The net system also includes the linear observer that is implemented as part of the detector. The impulse response $\Gamma(t)$ can be found in closed form for a given set of parameters of cantilever-observer system [11].

Channel Noise ($n(t)$): The measurement noise (from the imprecision in measuring the cantilever position) and thermal noise (from modeling mismatches) can be modeled by a single zero mean white Gaussian noise process ($n(t)$) with power spectral density equal to V .

The continuous time innovation output $e(t)$ becomes,

$$e(t) = \sum_{k=0}^{Nq-1} \nu_k(\bar{a}) \Gamma(t - kT_c) + n(t) = s(t, \bar{\nu}(\bar{a})) + n(t),$$

where $s(t, \bar{\nu}(\bar{a})) = \sum_{k=0}^{Nq-1} \nu_k(\bar{a}) \Gamma(t - kT_c)$ and $\bar{\nu}(\bar{a}) = (\nu_0(\bar{a}), \nu_1(\bar{a}) \dots \nu_{Nq-1}(\bar{a}))$. The sequence of impact values $\bar{\nu}_i$ is assumed to follow a Markovian model as explained above, $\Gamma(t)$ is the channel impulse response and $n(t)$ is a zero mean white Gaussian noise process.

A. Sufficient Statistics for Channel model

A set of sufficient statistics for the channel model is derived in this section. Given the probabilistic model on ν and finite bit sequence (\bar{a}), an orthogonal information lossless discretization of $e(t)$ by expansion over an orthonormal finite-dimensional basis with dimension \tilde{N} can be achieved where \tilde{N} orthonormal basis functions span the signal space formed by $s(t, \bar{\nu}(\bar{a}))$. The discretized innovation by expanding $e(t)$ over \tilde{N} orthonormal basis functions is given by, $\bar{\epsilon} = \bar{s}(\bar{\nu}(\bar{a})) + \bar{n}$, where $\bar{\epsilon} = (\epsilon_0, \epsilon_1 \dots \epsilon_{\tilde{N}})$, $\bar{s}(\bar{\nu}(\bar{a})) = (s_0, s_1 \dots s_{\tilde{N}})$, $\bar{n} = (n_0, n_1 \dots n_{\tilde{N}})$ and $\bar{n} \sim N(0, VI_{\tilde{N} \times \tilde{N}})$ where $I_{\tilde{N} \times \tilde{N}}$ stands for $\tilde{N} \times \tilde{N}$ identity matrix. The maximum likelihood estimate of the bit sequence can be found as $\hat{\bar{a}} = \arg \max_{\bar{a} \in \{0,1\}^N} f(\bar{\epsilon}|\bar{a})$ where $\hat{\bar{a}} = (\hat{a}_0, \hat{a}_1 \dots \hat{a}_{N-1})$ is the estimated bit sequence and f denotes a pdf. The term $f(\bar{\epsilon}|\bar{a})$ can be further simplified as,

$$\begin{aligned} f(\bar{\epsilon}|\bar{a}) &= \int_{\bar{\nu}} f(\bar{\epsilon}|\bar{a}, \bar{\nu}) f(\bar{\nu}|\bar{a}) d\bar{\nu} = \int_{\bar{\nu}} \frac{1}{(2\pi V)^{\frac{\tilde{N}}{2}}} \\ &\times \exp \frac{-\|\bar{\epsilon} - \bar{s}(\bar{\nu}(\bar{a}))\|^2}{2V} f(\bar{\nu}|\bar{a}) d\bar{\nu} = \frac{1}{(2\pi V)^{\frac{\tilde{N}}{2}}} \exp \frac{-\|\bar{\epsilon}\|^2}{2V} \\ &\times \int_{\bar{\nu}} \exp \frac{-(\|\bar{s}(\bar{\nu}(\bar{a}))\|^2 - 2\bar{\epsilon}^T \bar{s}(\bar{\nu}(\bar{a})))}{2V} f(\bar{\nu}|\bar{a}) d\bar{\nu} \end{aligned}$$

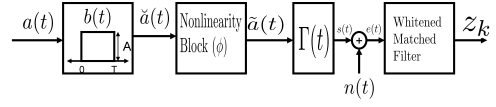


Fig. 4. Discretized channel model with whitened matched filter

where $\|\cdot\|^2$ denotes Euclidean norm, $f(\bar{\epsilon}|\bar{a}, \bar{\nu})$ and $f(\bar{\nu}|\bar{a})$ denote the respective conditional pdf's and $\bar{\nu} = (\nu_0, \nu_1 \dots \nu_{Nq-1})$. The correlation between $\bar{\epsilon}$ and $\bar{s}(\bar{\nu}(\bar{a}))$ can be equivalently expressed as an integral over time because of the discretization procedure. We have, $\bar{\epsilon}^T \bar{s}(\bar{\nu}(\bar{a})) = \bar{\nu}^T \bar{z}'$ where $z'_k = \int_{-\infty}^{\infty} e(t) \Gamma(t - kT_c) dt$ for $0 \leq k \leq Nq - 1$ is the output of a matched filter $\Gamma(-t)$ with input $e(t)$ sampled at $t = kT_c$, $\bar{\nu} = (\nu_0, \nu_1 \dots \nu_{Nq-1})$ and $\bar{z}' = (z'_0, z'_1 \dots z'_{Nq-1})$. $f(\bar{\epsilon}|\bar{a})$ can now be written as,

$$\begin{aligned} f(\bar{\epsilon}|\bar{a}) &= \underbrace{\frac{1}{(2\pi V)^{\frac{\tilde{N}}{2}}} \exp \frac{-\|\bar{\epsilon}\|^2}{2V}}_{h(\bar{\epsilon})} \\ &\times \underbrace{\int_{\bar{\nu}} \exp \frac{-\|\bar{s}(\bar{\nu}(\bar{a}))\|^2}{2V} \exp \frac{\bar{\nu}^T \bar{z}'}{V} f(\bar{\nu}|\bar{a}) d\bar{\nu}}_{\mathfrak{F}(\bar{z}'|\bar{a})} \end{aligned}$$

Thus $f(\bar{\epsilon}|\bar{a})$ can be factorized into $h(\bar{\epsilon})$ (dependent only on $\bar{\epsilon}$) and $\mathfrak{F}(\bar{z}'|\bar{a})$ (for a given \bar{a} dependent only on \bar{z}'). Using the Fisher-Neyman factorization theorem [3], it follows that \bar{z}' is a vector of sufficient statistics for the detection process. From the definition of sufficient statistics, we can claim, $\frac{f(\bar{\epsilon}|\bar{a})}{f(\bar{z}'|\bar{a})} = \mathcal{C}$, where \mathcal{C} is a constant independent of \bar{a} . Thus the detection problem can be reformulated as, $\hat{\bar{a}} = \arg \max_{\bar{a} \in \{0,1\}^N} f(\bar{z}'|\bar{a})$. The bit detection problem depends only on the matched filter outputs (\bar{z}'). These matched filter outputs z'_k for $0 \leq k \leq Nq - 1$ can be further simplified as, $z'_k = \sum_{k_1=0}^{Nq-1} \nu_{k_1}(\bar{a}) h'_{k-k_1} + n'_k$, where $h'_{k-k_1} = \int_{-\infty}^{\infty} \Gamma(t - kT_c) \Gamma(t - k_1T_c) dt$ and $n'_k = \int_{-\infty}^{\infty} n(t) \Gamma(t - kT_c) dt$. A whitening matched filter can be determined to whiten output noise n'_k [10]. We shall denote the discretized output of whitened matched filter shown in Figure 4 as z_k , such that $z_k = \sum_{k_1=0}^I \nu_{k-k_1}(\bar{a}) h_{k_1} + n_k$, where the filter $\{h_k\}_{k=0,1,\dots,I}$ denotes the effect of the whitened matched filter and the sequence $\{n_k\}$ represents Gaussian noise with variance V .

B. Viterbi Detector Design

Note that the outputs of the whitened matched filter \bar{z} , continue to remain sufficient statistics for the detection problem. Therefore, we can reformulate the detection strategy as,

$$\begin{aligned} \hat{\bar{a}} &= \arg \max_{\bar{a} \in \{0,1\}^N} f(\bar{z}|\bar{a}) \\ &= \arg \max_{\bar{a} \in \{0,1\}^N} \prod_{i=0}^{N-1} f(\bar{z}_i|\bar{a}, \bar{z}_0^{i-1}) \end{aligned} \quad (2)$$

where $\bar{z} = [z_0 \ z_1 \dots z_{Nq-1}]^T$. Let \bar{z}_i be the received output vector corresponding to the i^{th} input bit i.e. $\bar{z}_i = [z_{iq} \ z_{iq+1} \dots z_{(i+1)q-1}]^T$ and $\bar{z}_0^{i-1} = [z_0^T \ z_1^T \dots z_{i-1}^T]^T$. In our model, the channel is characterized by finite impulse response of length I i.e. $h_i = 0$ for $i < 0$ and $i > I$. In this work we assume that $I \leq m_I q$ i.e. the inter-symbol-interference (ISI) length in terms of q hits is equal to m_I . Let m be the inherent memory of the system (see (1)). The length of channel response is known which means m_I is known but the value

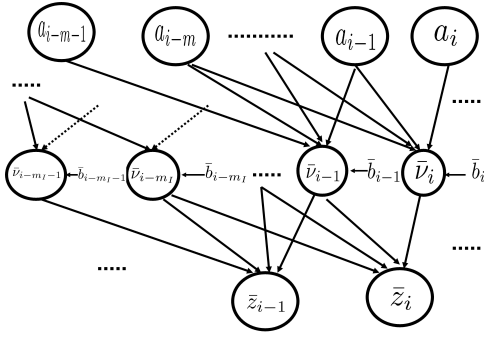


Fig. 5. Dependency graph for the model with $I = m_I q$ and m is the inherent memory of the system

of m can't be found because m is the inherent memory of the system and depends on the experimental parameters of the system. In the experimental results section, we describe how we estimate the value of m from experimental data. The received output vector \bar{z}_i can now be written as,

$$\bar{z}_i = \begin{pmatrix} h_I & . & . & h_0 & 0 & . & . & 0 \\ 0 & h_I & . & . & h_0 & 0 & . & 0 \\ . & . & . & . & . & . & . & . \\ 0 & . & . & 0 & h_I & . & . & h_0 \end{pmatrix} \begin{pmatrix} \nu_{iq-I} \\ \nu_{1+iq-I} \\ \vdots \\ \nu_{(i+1)q-1} \end{pmatrix} + \bar{n}_i$$

$$= H\bar{\nu}_{i-m_I}^i + \bar{n}_i$$

where $\bar{\nu}_i = [\nu_{iq} \ \nu_{iq+1} \dots \nu_{(i+1)q-1}]^T$, $\bar{\nu}_{i-m_I}^i = [\bar{\nu}_{i-m_I}^T \dots \bar{\nu}_i^T]^T$, $\bar{n}_i = [n_{iq} \ n_{1+iq} \dots n_{(i+1)q-1}]^T$.

We now simplify the factorization in (2) so that decoding can be made tractable. We construct the dependency graph of the concerned quantities which is shown in Figure 5. Using the Bayes ball algorithm [14], we conclude that

$$f(\bar{z}_i | \bar{\nu}_{i-m_I}^i, \bar{a}, \bar{z}_0^{i-1}) = f(\bar{z}_i | \bar{\nu}_{i-m_I}^i), \quad (3)$$

$$f(\bar{\nu}_{i-m_I} | \bar{a}, \bar{z}_0^{i-1}) = f(\bar{\nu}_{i-m_I} | a_0^{i-1}, \bar{z}_0^{i-1}), \quad (4)$$

$$f(\bar{\nu}_{i-k} | \bar{\nu}_{i-m_I}^{i-k-1}, \bar{a}, \bar{z}_0^{i-1}) = f(\bar{\nu}_{i-k} | \bar{\nu}_{i-m_I}^{i-k-1}, a_0^{i-m_I-1}, a_{i-m-k}^{i-1}, \bar{z}_0^{i-1}), \forall 1 \leq k \leq m_I - 1 \quad (5)$$

$$f(\bar{\nu}_i | \bar{\nu}_{i-m_I}^{i-1}, \bar{a}, \bar{z}_0^{i-1}) = f(\bar{\nu}_i | a_{i-m}^i) \quad (6)$$

where $a_0^{i-1} = [a_0 \ a_1 \ \dots \ a_{i-1}]$. Although the conditional pdf $f(\bar{\nu}_{i-m_I} | \bar{a}, \bar{z}_0^{i-1})$ and $f(\bar{\nu}_{i-k} | \bar{\nu}_{i-m_I}^{i-k-1}, \bar{a}, \bar{z}_0^{i-1})$ depend on the entire past, we assume that the dependence is rapidly decreasing. This is observed in simulation and experimental data as well. We make the following assumptions on this dependence,

$$f(\bar{\nu}_{i-m_I} | a_0^{i-1}, \bar{z}_0^{i-1}) \approx f(\bar{\nu}_{i-m_I} | a_{i-m-m_I}^{i-1}, \bar{z}_0^{i-1}) \quad (7)$$

$$f(\bar{\nu}_{i-k} | \bar{\nu}_{i-m_I}^{i-k-1}, a_0^{i-m_I-1}, a_{i-m-k}^{i-1}, \bar{z}_0^{i-1}) \approx f(\bar{\nu}_{i-k} | \bar{\nu}_{i-m_I}^{i-k-1}, a_{i-m-k-m}^{i-1}, \bar{z}_0^{i-1}), \forall 1 \leq k \leq m_I - 1 \quad (8)$$

i.e. the dependence is restricted to only the immediate neighbors in the dependency graph. Using the above assumptions and dependency graph results, $f(\bar{z}_i | \bar{a}, \bar{z}_0^{i-1})$ can be further

simplified as,

$$\begin{aligned} f(\bar{z}_i | \bar{a}, \bar{z}_0^{i-1}) &= \int f(\bar{z}_i | \bar{\nu}_{i-m_I}^i, \bar{a}, \bar{z}_0^{i-1}) f(\bar{\nu}_{i-m_I}^i | \bar{a}, \bar{z}_0^{i-1}) d\bar{\nu}_{i-m_I}^i \\ &= \int f(\bar{z}_i | \bar{\nu}_{i-m_I}^i, \bar{a}, \bar{z}_0^{i-1}) f(\bar{\nu}_{i-m_I} | \bar{a}, \bar{z}_0^{i-1}) \\ &\quad \cdot \Pi_{k=1}^{m_I-1} f(\bar{\nu}_{i-k} | \bar{\nu}_{i-m_I}^{i-k-1}, \bar{a}, \bar{z}_0^{i-1}) f(\bar{\nu}_i | \bar{\nu}_{i-m_I}^{i-1}, \bar{a}, \bar{z}_0^{i-1}) d\bar{\nu}_{i-m_I}^i \\ &= \int f(\bar{z}_i | \bar{\nu}_{i-m_I}^i) f(\bar{\nu}_{i-m_I} | a_0^{i-1}, \bar{z}_0^{i-1}) \Pi_{k=1}^{m_I-1} f(\bar{\nu}_{i-k} | \bar{\nu}_{i-m_I}^{i-k-1}, \\ &\quad a_0^{i-m_I-1}, a_{i-m-k}^{i-1}, \bar{z}_0^{i-1}) f(\bar{\nu}_i | a_{i-m}^i) d\bar{\nu}_{i-m_I}^i \text{ (Using (3),(4),(5),(6))} \\ &= \int f(\bar{z}_i | \bar{\nu}_{i-m_I}^i) f(\bar{\nu}_{i-m_I} | a_{i-m-m_I}^{i-1}, \bar{z}_0^{i-1}) \Pi_{k=1}^{m_I-1} f(\bar{\nu}_{i-k} | \\ &\quad \bar{\nu}_{i-m_I}^{i-k-1}, a_{i-m-k-m}^{i-1}, \bar{z}_0^{i-1}) f(\bar{\nu}_i | a_{i-m}^i) d\bar{\nu}_{i-m_I}^i \text{ (Using (7),(8))} \\ &= f(\bar{z}_i | a_{i-m-m_I}^i, \bar{z}_0^{i-1}). \end{aligned}$$

By defining a state $S_i = a_{i-m-m_I+1}^i$, this can be further expressed as $f(\bar{z}_i | S_i, S_{i-1}, \bar{z}_0^{i-1})$. Again using Bayes ball algorithm, we conclude that

$$f(\bar{z}_{i-m_I}^i | \bar{\nu}_{i-2m_I}^i, a_{i-m-m_I}^i) = f(\bar{z}_{i-m_I}^i | \bar{\nu}_{i-2m_I}^i), \quad (9)$$

$$\begin{aligned} \Pi_{k=1}^{2m_I-1} f(\bar{\nu}_{i-2m_I+k} | \bar{\nu}_{i-2m_I}^{i-2m_I+k-1}, a_{i-m-m_I}^i) \\ = \Pi_{k=1}^{m_I-1} f(\bar{\nu}_{i-2m_I+k} | \bar{\nu}_{i-2m_I}^{i-2m_I+k-1}, a_{i-m-m_I}^i) \\ \cdot \Pi_{k=m_I}^{2m_I-1} f(\bar{\nu}_{i-2m_I+k} | a_{i-2m_I-m+k}^{i-2m_I+k}), \end{aligned} \quad (10)$$

$$f(\bar{\nu}_i | \bar{\nu}_{i-2m_I}^{i-1}, a_{i-m-m_I}^i) = f(\bar{\nu}_i | a_{i-m}^i). \quad (11)$$

The pdf of $\bar{z}_{i-m_I}^i = [\bar{z}_{i-m_I}^T \dots \bar{z}_i^T]^T$ given current state S_i and previous state S_{i-1} is given by,

$$\begin{aligned} f(\bar{z}_{i-m_I}^i | S_i, S_{i-1}) &= f(\bar{z}_{i-m_I}^i | a_{i-m-m_I}^i) \\ &= \int f(\bar{z}_{i-m_I}^i | \bar{\nu}_{i-2m_I}^i, a_{i-m-m_I}^i) f(\bar{\nu}_{i-2m_I}^i | a_{i-m-m_I}^i) d\bar{\nu}_{i-2m_I}^i \\ &= \int f(\bar{z}_{i-m_I}^i | \bar{\nu}_{i-2m_I}^i, a_{i-m-m_I}^i) f(\bar{\nu}_{i-2m_I} | a_{i-m-m_I}^i) \\ &\quad \cdot \Pi_{k=1}^{2m_I-1} f(\bar{\nu}_{i-2m_I+k} | \bar{\nu}_{i-2m_I}^{i-2m_I+k-1}, a_{i-m-m_I}^i) \\ &\quad \cdot f(\bar{\nu}_i | \bar{\nu}_{i-2m_I}^{i-1}, a_{i-m-m_I}^i) d\bar{\nu}_{i-2m_I}^i \\ &= \int f(\bar{z}_{i-m_I}^i | \bar{\nu}_{i-2m_I}^i) f(\bar{\nu}_{i-2m_I} | a_{i-m-m_I}^i) \Pi_{k=1}^{m_I-1} \\ &\quad \cdot f(\bar{\nu}_{i-2m_I+k} | \bar{\nu}_{i-2m_I}^{i-2m_I+k-1}, a_{i-m-m_I}^i) \Pi_{k=m_I}^{2m_I-1} f(\bar{\nu}_{i-2m_I+k} | \\ &\quad a_{i-2m_I-m+k}^{i-2m_I+k}) f(\bar{\nu}_i | a_{i-m}^i) d\bar{\nu}_{i-2m_I}^i \text{ (Using (9),(10),(11))} \end{aligned}$$

where the last step is obtained using results from dependency graph and all the terms in the last step except $\Pi_{k=1}^{m_I-1} f(\bar{\nu}_{i-2m_I+k} | \bar{\nu}_{i-2m_I}^{i-2m_I+k-1}, a_{i-m-m_I}^i)$ and $f(\bar{\nu}_{i-2m_I} | a_{i-m-m_I}^i)$ are Gaussian distributed. This implies that the pdf of $\bar{z}_{i-m_I}^i$ given (S_i, S_{i-1}) is not exactly Gaussian distributed. If the number of states in the detector is increased it can be modeled as a Gaussian, but this increases the complexity. In order to keep the decoding tractable we make the assumption that $f(\bar{z}_{i-m_I}^i | S_i, S_{i-1})$ is Gaussian i.e.

$$f(\bar{z}_{i-m_I}^i | S_i, S_{i-1}) \sim N(\bar{\mathcal{Y}}(S_i, S_{i-1}), \mathcal{C}(S_i, S_{i-1}))$$

where $\bar{\mathcal{Y}}(S_i, S_{i-1})$ is the mean and $\mathcal{C}(S_i, S_{i-1})$ is the covariance. With our state definition, we can reformulate the detection problem as a maximum likelihood state sequence

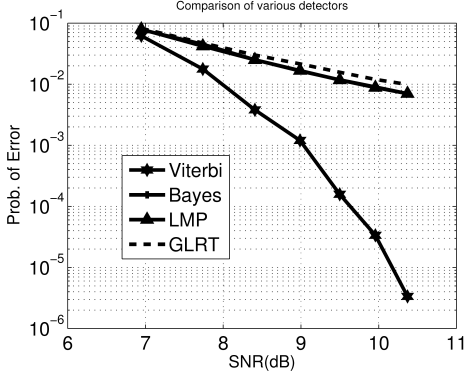


Fig. 6. Comparison of various detectors for simulation data. The Bayes curve is not visible in the graph as it coincides with the LMP curve.

detection problem [2],

$$\begin{aligned}
 \hat{\bar{S}} &= \arg \max_{\bar{S}} f(\bar{z}|\bar{S}) = \arg \max_{\bar{S}} \prod_{i=0}^{N-1} f(\bar{z}_i|\bar{S}, \bar{z}_0 \dots \bar{z}_{i-1}) \\
 &= \arg \max_{\bar{S}} \prod_{i=0}^{N-1} f(\bar{z}_i|S_i, S_{i-1}, \bar{z}_{i-m_I}^{i-1}) \\
 &= \arg \max_{\bar{S}} \prod_{i=0}^{N-1} \frac{f(\bar{z}_{i-m_I}^i|S_i, S_{i-1})}{f(\bar{z}_{i-m_I}^{i-1}|S_i, S_{i-1})} \\
 &= \arg \min_{\bar{S}} \sum_{i=0}^{N-1} \log \frac{|c(S_i, S_{i-1})|}{|c(S_i, S_{i-1})|} + (\bar{z}_{i-m_I}^i - \bar{y}(S_i, S_{i-1}))^T \\
 &\quad \cdot c(S_i, S_{i-1})^{-1} (\bar{z}_{i-m_I}^i - \bar{y}(S_i, S_{i-1})) - (\bar{z}_{i-m_I}^{i-1} \\
 &\quad - \bar{y}(S_i, S_{i-1}))^T c(S_i, S_{i-1})^{-1} (\bar{z}_{i-m_I}^{i-1} - \bar{y}(S_i, S_{i-1}))
 \end{aligned}$$

where $\hat{\bar{S}}$ is the estimated state sequence, $c(S_i, S_{i-1})$ is the upper $m_I q \times m_I q$ principal minor of $\mathcal{C}(S_i, S_{i-1})$ and $\bar{y}(S_i, S_{i-1})$ collects the first $m_I q$ elements of $\bar{Y}(S_i, S_{i-1})$. It is assumed that the first state is known. With the metric given above, Viterbi decoding can be applied to get the maximum likelihood state sequence.

C. LMP, GLRT and Bayes Detector

In [12], the hit detection algorithm is proposed which doesn't consider the modeling of channel memory and works well only when the hits are sufficiently apart. In [11], various detectors for hit detection like locally most powerful (LMP), generalized likelihood ratio test (GLRT) and Bayes detector are presented. These detectors also ignore the inherent memory in the channel and perform detection of single hits. Subsequently a majority type rule is used for bit detection.

IV. SIMULATION RESULTS

We performed simulations with the following parameters. The first resonant frequency of the cantilever $f_0 = 63.15$ KHz, quality factor $Q = 206$, the number of hits in high bit duration is equal to 13 i.e. $q = 13$, the cantilever forcing is chosen such that the cantilever amplitude is 24 nm (without any interaction with media), tip-media separation is 28 nm, discretized thermal and measurement noise variance are 0.1 and 0.001 respectively. With these thermal and measurement noise values, a Kalman observer is designed and the length of the channel impulse response (I) is approximately 24 for designed observer which means m_I is equal to 2. Bit error rate (BER) will improve by taking higher values of the inherent memory of the system (m) but it will increase complexity of

detector. Considering the tradeoff between BER and m , we are using $m = 1$ for simulation data. We used a topographic profile where high and low regions denote the bit '1' and '0' respectively and the bit sequence is generated randomly. There are 13 hits when the bit is '1'. The simulation was performed with the above parameters using the Simulink model that mimics the experimental station that provides a qualitative as well as a quantitative match to the experimental data. The innovations were obtained at the output of the observer for different tip-media interaction. We define the system SNR as tip media interaction (nm) divided by total noise variance.

In Figure 6, we compare the results of four different detectors. The locally most powerful (LMP), generalized likelihood ratio test (GLRT) and Bayes detector proposed in [11] perform hit detection, as against bit detection. The minimum probability of error for all detectors decreases as the tip-media interaction increases because hits become harder on media if tip-media interaction is increased which makes detection easier. The Viterbi detector gives best performance among all detectors because it incorporates the Markovian property of ν in the metric used for detection. At an SNR of 10.4 dB the Viterbi detector has a BER of 3×10^{-6} as against the LMP detector that has 7×10^{-3} .

V. EXPERIMENTAL RESULTS

In experiments, a cantilever with resonant frequency $f_0 = 71.78$ KHz and quality factor $Q = 67.55$ is oscillated near its resonant frequency. A freshly cleaved mica sheet is placed on top of a high bandwidth piezo. This piezo can position the media (mica sheet) in z-direction with respect to cantilever tip. A random sequence of bits is generated through a FPGA board and applied to the z-piezo. High level is equivalent to 1000 mV and represents bit '1' and low level is 0 V and represents bit '0' thus creating a pseudo media profile of 6 nm height. The bit width can be changed using FPGA controller. Thus we can change the bit width from 350 μs till 60 μs . The tip is engaged with the media at a single point and its instantaneous amplitude in response to its interaction with z piezo is monitored. The controller gain is kept sufficiently low such that the operation is effectively in open loop. The gain is sufficient to cancel piezo drift and maintain a certain level of tip-media interaction. An observer is implemented in another FPGA board which is based on the plant's free air model and takes plant dither and deflection signals as its input and gives out innovation signal at the output. The innovation signal is used to detect bits by comparing various bit detection algorithms. The experiments were performed on Multimode AFM, from Veeco Instruments. Considering a bit width of 40 nm and the amount of time for scanning of 60 μs gives a tip velocity equal to $2/3 \times 10^{-3}$ m/sec. The total scan size is 100 micron which means the cantilever will take 0.15 seconds to complete one full scan. Read scan speed for this operation is 6.66 Hz. The read scan speed for different bit width can be found in a similar manner.

With above setup, experiments are performed for different bit widths varying from 60 μs to 300 μs . For 300 μs bit width, there are around 21 hits in high bit duration and Viterbi decoding is applied on the innovation signal obtained from experiment. For experimental model, I is approximately

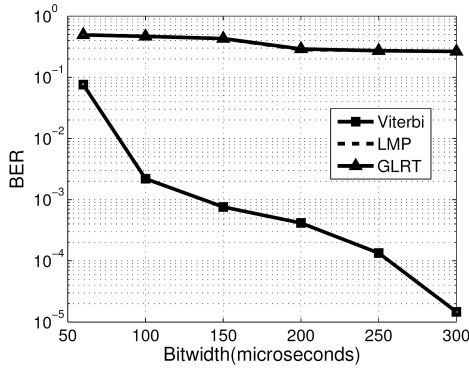


Fig. 7. BER for Viterbi, LMP and GLRT for different bit widths varying from 60 μ s to 300 μ s for experimental data. There is a very marginal difference between LMP and GLRT curve which is not visible in the graph but LMP does perform better than GLRT.

24 which means m_I is equal to 2. It is hard to estimate the inherent memory of the system (m) from experimental parameters. We have varied m from 0 to 2 and found different BER using these values of m . The total number of states in the Viterbi detector is 2^{m+m_I} . For $m \geq 1$, the improvement in BER is quite marginal as compared to the increased complexity of Viterbi decoding. Considering the tradeoff between the complexity of Viterbi decoding and m , we use $m = 1$ for which BER from Viterbi decoding is equal to 1×10^{-5} whereas BER from locally most powerful (LMP) test is 0.26. BER in the case of Viterbi decoding is quite less as compared to BER for usual thresholding detectors. If the bit width is decreased to 60 μ s which means there are around 4 hits in high bit duration, BER for Viterbi decoding is 7.56×10^{-2} whereas BER for LMP is 0.49 which means that LMP is doing almost no bit detection. As the bit width is decreased, there is more ISI between adjacent bits which increases BER. BER for all detectors and bit widths is shown in Figure 7. It is evident that Viterbi decoding gives remarkable results on experimental data as compared to LMP detector. Viterbi detector captures cantilever dynamics behaviour quite precisely in terms of mean and covariance matrix for different state transitions. Thresholding detectors like LMP and GLRT given in [11] perform very badly on experimental data. For bit sequence like '00001111', cantilever gets enough time to go into steady state in the beginning and hits quite hard on media when bit '1' comes after a long sequence of '0' bits. The likelihood ratio for LMP and GLRT rise significantly for the bit '1' which can be easily detected through thresholding. However a sequence of continuous '1' bits keeps the cantilever in steady state and the cantilever starts hitting mildly on media which means the likelihood ratio remains small for these bits. It is very likely that long sequence of '1' bits will not get detected by threshold detectors.

VI. CONCLUSIONS AND FUTURE WORK

We presented the dynamic mode operation of a cantilever probe with a high quality factor and demonstrated its applicability to a high-density probe storage system. The system is modeled as a communication system by modeling the cantilever interaction with media. The bit detection problem is solved by posing it as a maximum likelihood sequence detection followed by Viterbi decoding. Simulation and exper-

imental results show that Viterbi detector outperforms all the detectors and gives remarkably low BER. For dynamic mode operation with high quality factors to be practical for data storage applications, it is evident that the modeling paradigm developed is crucial as the performance of other methods does not meet the stringent requirements of data storage metrics.

Constrained codes are used in almost all forms of storage including magnetic hard drives. It is quite certain that constrained codes will help the detection scheme with some loss of rate. In future work, the trade-off between the rate loss and detector performance will be researched. In experimental data, some amount of jitter is inevitably present which is well handled by our algorithm as the jitter is smaller than the bit width chosen. But if the jitter is in the order of bit width, which may be the case at very high densities we need to apply more advanced modeling and detection techniques which will be part of future work.

REFERENCES

- [1] Seiji Akita, Hidehiro Nishijima, Takayoshi Kishida, and Yoshikazu Nakayama. Nanoindentation of polycarbonate using carbon nanotube tip. *International Microprocesses and Nanotechnology Conference*, pages 228 – 229, 2000.
- [2] Kavcic Aleksandar and Jose M. F. Moura. The Viterbi Algorithm and Markov Noise Memory. *IEEE Trans. on Info. Th.*, 46, Issue: 1:291–301, 2000.
- [3] G. Casella and R. Berger. *Statistical Inference*. Duxbury Thomson Learning, second edition, 2002.
- [4] B.W. Chui, H.J. Mamin, B.D. Terris, D. Rugar, and T.W. Kenny. Sidewall-implanted dual-axis piezoresistive cantilever for afm data storage readback and tracking. pages 12–17, Jan 1998.
- [5] P. Baechtold A. Sebastian H. Pozidis D. R. Sahoo, W. Haeberle and E. Eleftheriou. On intermittent-contact mode sensing using electrostatically-actuated micro-cantilevers with integrated thermal sensors. *Proceeding of the American Control Conference*, pages 2034 – 2039, June 2008.
- [6] U. Dürig. Fundamentals of micromechanical thermoelectric sensors. *Journal of Applied Physics*, 98:044, 2005.
- [7] Fedor N Dzegilenko, Deepak Srivastava, and Subhash Saini. Nanoscale etching and indentation of a silicon(001) surface with carbon nanotube tips. *Nanotechnology*, 10:253257, 1999.
- [8] E. Eleftheriou et al. Millepede - A MEMS-based Scanning-Probe Data-Storage System. *IEEE Trans. on Magnetics*, 39, no. 2:938–945, 2003.
- [9] E. Eleftheriou et al. A nanotechnology-based approach to data storage. In *VLDB '2003: Proceedings of the 29th international conference on Very large data bases*, pages 3–7. VLDB Endowment, 2003.
- [10] J. Forney, G. Maximum-likelihood sequence estimation of digital sequences in the presence of intersymbol interference. *IEEE Trans. on Info. Th.*, 18, Issue: 3:363 – 378, 1972.
- [11] N. Kumar, P. Agarwal, A. Ramamoorthy, and M. Salapaka. Channel modeling and detector design for dynamic mode high density probe storage. In *42nd Conference on Information Sciences and Systems*. IEEE, 2008.
- [12] D. R. Sahoo, A. Sebastian, and M. V. Salapaka. Harnessing the transient signals in atomic force microscopy. *International Journal of Robust and Nonlinear Control, Special Issue on Nanotechnology and Micro-biology*, 15:805–820, 2005.
- [13] A. Sebastian, M. V. Salapaka, D. Chen, and J. P. Cleveland. Harmonic and power balance tools for tapping-mode atomic force microscope. *Journal of Applied Physics*, 89 (11):6473–6480, June 2001.
- [14] R. D. Shachter. Bayes-Ball: The Rational Pastime (for Determining Irrelevance and Requisite Information in Belief Networks and Influence Diagrams). In *Uncertainty in Artificial Intelligence: Proceedings of the Fourteenth Conference*, pages 480–487, 1998.
- [15] P. Vettiger, G. Cross, M. Despont, U. Drechsler, U. Durig, B. Gotsmann, W. Haberele, M. A. Lantz, H. Rothuizen, R. Stutz, and G. Binnig. The millipede-nanotechnology entering data storage. *IEEE Transactions on Nanotechnology*, 1(1), 2002.
- [16] Q. Zhong, D. Inniss, K. Kjoller, and V B Elings. Fractured polymer/silica fiber surface studied by tapping mode atomic force microscopy. *Surface Science Letters*, 290:L688–L692, 1993.